Inorganic Chemistry

Article

pubs.acs.org/IC

Alkynyl-naphthalimide Fluorophores: Gold Coordination Chemistry and Cellular Imaging Applications

Emily E. Langdon-Jones,[†] David Lloyd,[‡] Anthony J. Hayes,[‡] Shane D. Wainwright,[‡] Huw J. Mottram,[§] Simon J. Coles,[∥] Peter N. Horton,[∥] and Simon J. A. Pope*[,†]

[†]School of Chemistry, Main Building, Cardiff University, Cardiff CF10 3AT, United Kingdom

[‡]School of Biosciences, Main Building, Cardiff University, Cardiff CF10 3AT, United Kingdom

[§]School of Pharmacy, Redwood Building, Cardiff University, Cardiff CF10 3NB, United Kingdom

[∥]UK National Crystallographic Service, Chemistry, Faculty of Natural and Environmental Sciences, University of Southampton, Highfield, Southampton SO17 1BJ, United Kingdom

Supporting Information

ABSTRACT: A range of fluorescent alkynyl-naphthalimide fluorophores has been synthesized and their photophysical properties examined. The fluorescent ligands are based upon a 4-substituted 1,8-naphthalimide core and incorporate structural variations (at the 4-position) to tune the amphiphilic character: chloro (**L1**), 4-[2-(2-aminoethoxy)ethanol] (**L2**), 4-[2-(2-methoxyethoxy)ethylamino] (**L3**), piperidine (**L4**), morpholine (**L5**), 4-methylpiperidine (**L6**), and 4-piperidone ethylene ketal (**L7**) variants. The amino-substituted species (**L2**–**L7**) are fluorescent in the visible region at around 517–535 nm through a naphthalimide-localized intramolecular charge transfer (ICT), with appreciable Stokes' shifts of ca. 6500 cm^{-1} and lifetimes up to 10.4 ns. Corresponding two-coordinate Au(I) complexes [Au(L)(PPh_3)] were isolated, with X-ray structural studies revealing the expected coordination mode via the alkyne donor. The Au(I) complexes retain the visible fluorescence associated with the coordinated alkynyl-naphthalimide ligand. The ligands and complexes were investigated for their cytotoxicity across a range of cell lines (LOVO, MCF-7, A549, PC3, HEK) and their potential as cell imaging agents for HEK (human embryonic kidney) cells and *Spironucleus vortens* using confocal fluorescence microscopy. The images reveal that these fluorophores are highly compatible with fluorescence microscopy and show some clear intracellular localization patterns that are dependent upon the specific nature of the naphthalimide substituent.

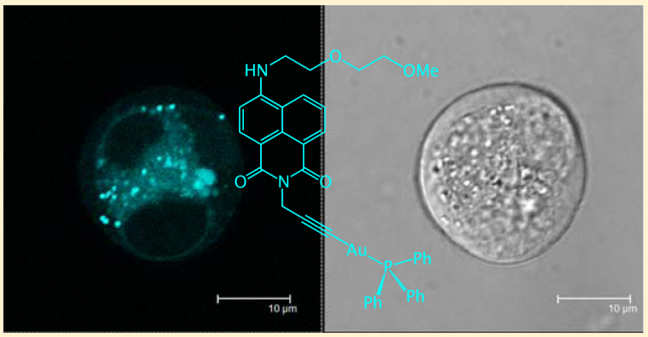

INTRODUCTION

The use of gold-based compounds in medicinal chemistry is known as chrysotherapy,[1] and compounds such as sodium aurothiomalate and auranofin have been successfully used to treat inflammatory autoimmune conditions like rheumatoid arthritis.[2] Unraveling the biological action of such species is very challenging,[3] with the inhibition of cathepsin B activity (via targeting of cysteine proteases),[4] and the interuption of oxidative stress regulation in cells through the inhibition of the enzyme thioredoxin reductase (TrxR),[5] one of the pharmacologically important pathways. However, the toxicity from many Au(I) complexes, and the unclear biological mode of action of such compounds[6] in the treatment of rheumatoid arthritis, still detract from the established medical benefits.[7] Many gold compounds also show antiproliferative properties, but the antitumor activity is not well understood.[8]

A detailed understanding into the mechanisms of biological action informs the rational design of new therapeutics.[9] However, elucidating the cellular uptake and intracellular distribution of Au(I) complexes is challenging. The developments in the cellular imaging of Au(I) complexes can be embodied in two strategies: (i) the use of analytical techniques that allow elemental isotopic (e.g., ^{197}Au) composition to be mapped; and (ii) the functionalization of Au(I) complexes with fluorescent labels compatible with confocal fluorescence microscopy. It is important to note that the known therapeutic gold complexes sodium aurothiomalate and auranofin do not possess the necessary luminescence properties to allow confocal fluorescence microscopy.

In this context, and in contrast to better known d^{10} (e.g., based on Ru(II),[11] Re(I),[12] Ir(III)[13]) and d^8 (predominantly Pt(II))[14] lumophores, which have been more widely applied to cellular imaging, only a small handful of studies have explored the cellular uptake and distribution of various (d^{10}) Au(I) complexes using confocal fluorescence microscopy. Linear Au(I) complexes incorporating an ancillary phosphine (with varying alkyl/aryl groups) and a thiolated fluorophoric ligand,

Received: April 28, 2015
Published: June 18, 2015

DOI: 10.1021/acs.inorgchem.5b00954
Inorg. Chem. 2015, 54, 6606–6615

giving [Au(PR_3)(S-Nap)] (where S-Nap = 4-mercapto-1,8-naphthalic anhydride or *N*-(*N*′,*N*′-dimethylaminoethyl)-1,8-naphthalimide-4-sulfide) have been reported,[15] and confocal fluorescence microscopy imaging of MCF7 cells showed localization in cell nuclei. Supporting cytotoxicity studies showed IC_{50} values of 1.1−3.7 μM for MCF-7 cells, which were comparable to those of auranofin (IC_{50} = 1.1 μM) and cisplatin (IC_{50} = 2.0 μM); the free 1,8-naphthalimide ligands were also cytotoxic (IC_{50} = 1.9−4.6 μM).[16]

Water-soluble cyclophane-bridged *N*-heterocyclic carbene complexes of Au(I) have also found applicability to confocal fluorescence microscopy.[17] The emission properties of the dimetallic Au(I) complexes were biocompatible, and cell imaging with RAW264.8 cells revealed good uptake and lysosomal localization with a mild cytotoxicity (IC_{50} = 52 μM). Recently, alkyne-coordinated Au(I) complexes have been shown to selectively target TrxR.[18] In earlier work, we have shown that fluorescent alkynyl-functionalized anthraquinone ligands and their corresponding mono- and dimetallic Au(I) complexes can be applied to cellular studies.[19] Confocal fluorescence microscopy revealed that all complexes showed good uptake (>80%) with MCF7 cells with general cytoplasmic staining, but limited evidence for any specific organelle localization.

With appropriate design, Au(I) complexes therefore have much to offer in the realm of cellular imaging, with the dual opportunities for therapeutic action.[20] Fluorescent Au(I) complexes that are based upon anthracenyl *N*-heterocyclic carbene (NHC) ligands have been shown to lead to oxidation of the thioredoxin system, while the anthracene fluorophore enables visualization of cellular distribution using fluorescence microscopy.[21] In related work, attachment of coumarin fluorophores to the NHC framework also allowed the study of the resultant Au(I) complexes, showing that they inhibit TrxR; fluorescence microscopy showed that the complexes can target the nuclear compartment in tumor cells.[22] Alkynyl derivatives of coumarin have also been described but may not possess the requisite luminescence properties for confocal fluorescence microscopy.[23] On the other hand, pairing Au(I) alkyne moieties with luminescent Re(I) can facilitate imaging, while suggesting cooperative behavior with respect to biological action.[24]

Here, we report our studies of a series of Au(I) complexes that incorporate highly fluorescent 4-substituted 1,8-naphthalimide chromophores coordinated to gold via a terminal propargyl donor. The 1,8-naphthalimide can be relatively easily functionalized in a stepwise manner allowing control over relevant physical properties such as solubility and photophysics.[25] The amino-substituted variants are known to possess charge transfer excited-state properties, which shift the absorption and emission profiles into the visible region while also imparting a useful (cf., confocal fluorescence microscopy) Stokes' shift (the difference between λ_{abs} and λ_{em}), and has led to these fluorophores now being explored in the context of fluorescence imaging of cells. In parallel, it is also important to note that 1,8-naphthalimide derivatives are of great interest in the context of DNA binding,[26] as well as their consideration in luminescent sensing platforms.[27]

In this Article, we describe the synthesis and characterization of seven new alkynyl-derived 1,8-naphthalimide fluorophores together with their linear two-coordinate Au(I) complexes. These new compounds were assessed for their comparative imaging capabilities, via the fluorescent naphthalimide ligand, using both human embryonic kidney (HEK) cells and the protistan fish parasite *Spironucleus vortens*. The results show that the specific functionalization of the 1,8-naphthalimide core determines the cellular uptake and distribution, with selected examples showing some outstanding imaging characteristics.

EXPERIMENTAL SECTION

X-ray Crystallography. Suitable crystals were selected and measured following a standard method[28] on a Rigaku AFC12 goniometer equipped with an enhanced sensitivity (HG) Saturn724+ detector mounted at the window of a FR-E+ SuperBright molybdenum rotating anode generator with VHF Varimax optics (70 μm focus) at 100 K. Cell determination, data collection, reduction, cell refinement, and absorption correction were carried out using CrystalClear-SM Expert 3.1b27.[29] Structures were solved using SUPERFLIP[30] and refined using SHELXL-2013.[31] CCDC reference numbers 1056114 (**L6**) and 1056115 (**Au-L6**) contain the supplementary crystallographic data for this Article. These data can be obtained free of charge from the Cambridge Crystallographic Data Centre via www.ccdc.cam.ac.uk/data_request/cif.

Cell Incubation and Confocal Microscopy. The human embryonic kidney cell line HEK293-EBNA (Invitrogen) was maintained in Dulbecco's Modification of Eagle Medium (DMEM) supplemented with 10% Foetal bovine serum, penicillin, streptomycin, and 250 ug/mL G418. Cells were detached by tapping the side of the tissue culture flasks. The homogeneous cell suspension was then distributed into 1 mL aliquots with each aliquot being subject to incubation with a different lumophore. Lumophores were initially dissolved in DMSO (5 mg/mL) before being added to the cell suspensions, final concentration 100 μg mL^{-1}, before incubation at 20 °C for 30 min. Cells were finally washed in phosphate buffer saline (PBS, pH 7.2), removing lumophore from the medium, then harvested by centrifugation (5 min, 800*g*) and mounted on a slide for imaging. *S. vortens*, ATCC 50386, trophozoites were maintained in Keister's modified TYI-S-33 medium without bile supplement as described previously.[32] Trophozoites were incubated at 23−24 °C and routinely subcultured at 24−48 h intervals by transferring 500 μL of an inverted log-phase culture into 10 mL of culture medium, leaving a 5 mL head space in 15 mL screw capped Falcon tubes (Greiner Bio-one). Parasite viability was monitored according to cell motility and visual estimation of cell density by phase contrast microscopy. When accurate cell counts were necessary, trophozoites were fixed in 1.5% formaldehyde and counted using an Improved Neubauer hemocytometer (Weber Scientific International). To ensure axenic maintenance, cultures were regularly monitored for microbial contamination by plating-out 100 μL of an exponentially growing culture on TYI-S-33 agar (0.5%, w/v) and incubating under the above conditions for 5 days. Cell preparations were viewed by epifluorescence and transmitted light (Nomarski differential interference contrast optics) using a Leica TCS SP2 AOBS confocal laser microscope (Leica, Germany) using ×63 or ×100 objectives. Excitation of the lumophore was at 405 nm, and detection was between 530 and 580 nm.

Cytotoxicity Assessment via MTT Assay. The cytotoxicity of the complexes was assessed using the colorimetic and quantitative MTT [3-(4,5-dimethylthiazol-2-yl)-2,5-diphenyltetrazolium bromide] assay, first reported by Mosmann.[33] Quantification was achieved using a multiwell scanning spectrophotometer and reported as an IC_{50} value.

Method for Cytotoxicity Analysis. Antitumor evaluation in MCF7, LOVO, A549, and PC3 cell lines was performed by MTT assay. Compounds were prepared as 0.1−100 mM stock solutions dissolved in DMSO and stored at −20 °C. Cells were seeded into 96-well microtiter plates at a density of 5×10^3 cells per well and allowed 24 h to adhere. Decimal compound dilutions were prepared in medium immediately prior to each assay (final concentration 0.1−100 μM). Experimental medium was DMEM + 10% FCS (PC3 and Lovo) or RPMI + 10% heat inactivated FCS (A549 and MCF7). Following 96 h compound exposure at 37 °C, 5% CO_2, MTT reagent (Sigma-Aldrich) was added to each well (final concentration 0.5 mg/mL). Incubation at 37 °C for 4 h allowed reduction of MTT by viable cells

DOI: 10.1021/acs.inorgchem.5b00954
Inorg. Chem. 2015, 54, 6606−6615

to an insoluble formazan product. MTT was removed and formazan solubilized by addition of 10% Triton X-100 in PBS. Absorbance was read on a Tecan Sunrise spectrophotometer at 540 nm as a measure of cell viability; thus inhibition relative to control was determined (IC_{50}) from four independent sets of data.

General. ^{1}H, $^{13}C\{^{1}H\}$, and $^{31}P\{^{1}H\}$ NMR spectra were recorded on an NMR-FT Bruker 400 MHz or Joel Eclipse 300 MHz spectrometer and recorded in $CDCl_3$. ^{1}H, $^{13}C\{^{1}H\}$, and $^{31}P\{^{1}H\}$ NMR chemical shifts (δ) were determined relative to residual solvent peaks with digital locking and are given in ppm. Low-resolution mass spectra were obtained by the staff at Cardiff University using a Waters LCT Premier XE mass spectrometer. High-resolution mass spectra were carried out at the EPSRC National Mass Spectrometry Facility at Swansea University. UV−vis studies were performed on a Jasco V-570 spectrophotometer as MeCN solutions (2.5 or 5×10^{-5} M). Photophysical data were obtained on a JobinYvon−Horiba Fluorolog spectrometer fitted with a JY TBX picoseconds photodetection module as MeCN solutions. Emission spectra were uncorrected, and excitation spectra were instrument corrected. Quantum yields used $[Ru(bpy)_3](PF_6)_2$ in aerated MeCN as a standard ($\Phi_{em} = 0.016$).[34] The pulsed source was a Nano-LED configured for 295 or 372 nm output operating at 1 MHz. Luminescence lifetime profiles were obtained using the JobinYvon−Horiba FluoroHub single photon counting module, and the data fits yielded the lifetime values using the provided DAS6 deconvolution software.

All reactions were performed with the use of vacuum line and Schlenk techniques. Reagents were commercial grade and were used without further purification. 2-(2-Methoxyethoxy)ethanamine was synthesized from commercially available 2-(2-methoxyethoxy)ethanol according to literature methods.[35] The $[AuCl(PPh_3)]$ precursor was obtained using well-established methods from the literature.[36]

Ligand Synthesis. *Synthesis of 4-Chloro-(N-(2-propyn-1-yl))-1,8-naphthalimide (**L1**).*[37] Propargyl amine (0.33 mL, 5.22 mmol) was added to a solution of 4-chloro-1,8-naphthalic anhydride (608 mg, 2.61 mmol) in EtOH (30 mL) and heated to just below reflux, under a nitrogen atmosphere for 8 h, followed by reduced heating at 50 °C for 16 h. Upon cooling the product was collected by filtration. Washing with EtOH (2×20 mL) and subsequent drying gave **L1** as an off-white solid. Yield: 634 mg, 2.35 mmol, 89.9%. ^{1}H NMR (400 MHz, $CDCl_3$): δ_H = 8.72 (d, 1H, $^{3}J_{HH}$ = 7.3 Hz), 8.64 (d, 1H, $^{3}J_{HH}$ = 8.5 Hz), 8.55 (d, 1H, $^{3}J_{HH}$ = 7.9 Hz), 7.90−7.84 (m, 2H), 4.95 (d, 2H, $^{4}J_{HH}$ = 2.5 Hz, CH_2), 2.20 (t, 1H, $^{4}J_{HH}$ = 2.5 Hz, C≡C*H*) ppm. UV−vis (MeCN): λ_{max} (ε/M^{-1} cm^{-1}) = 353 (11 600), 339 (13 700), 325(s) (10 100), 233 (41 100), 211 (16 500) nm. Emission (MeCN): λ_{em} (τ/ns) = 392 (3.0) nm.

*Synthesis of 4-(2-(2-Aminoethoxy)ethanol)-(N-(2-propyn-1-yl))-1,8-naphthalimide (**L2**).* **L1** (168 mg, 0.62 mmol) and 2-(2-aminoethoxy)ethanol (0.25 mL, 2.49 mmol) were stirred in DMSO (3 mL) at 90 °C under a nitrogen atmosphere for 16 h. The solution was then allowed to cool, and water (10 mL) was added, which induced precipitation of a yellow solid. The reaction mixture was then neutralized with 0.1 M HCl and the crude product extracted into dichloromethane, washed with water, dried over $MgSO_4$, and filtered. The solvent was reduced to a minimal volume, and precipitation was induced with diethyl ether, allowing subsequent filtration and drying to afford **L2** as an orange solid. Yield: 156 mg, 0.46 mmol, 74.0%. ^{1}H NMR (400 MHz, $CDCl_3$): δ_H = 8.71 (d, 1H, $^{3}J_{HH}$ = 6.4 Hz), 8.59 (d, 1H, $^{3}J_{HH}$ = 8.0 Hz), 8.27 (d, 1H, $^{3}J_{HH}$ = 7.6 Hz), 7.73 (app t, 1H, $^{3}J_{HH}$ = 7.6 Hz), 6.82 (d, 1H, $^{3}J_{HH}$ = 8.8 Hz), 6.00−5.94 (broad t, 1H, N*H*), 5.05 (d, 2H, $^{4}J_{HH}$ = 2.4 Hz, NCH_2), 4.02 (t, 2H, $^{3}J_{HH}$ = 5.6 Hz), 4.00−3.92 (broad m, 2H), 3.83−3.80 (m, 2H), 3.71 (app q, 2H, $^{3}J_{HH}$ = 5.2 Hz), 2.28 (t, 1H, $^{4}J_{HH}$ = 2.8 Hz, C≡C*H*) ppm. HRMS (ES+) found m/z 339.1343; $[C_{19}H_{18}N_2O_4+H]^+$ requires 339.1345. IR (solid): υ = 3360, 3261, 2356, 1742, 1680, 1629, 1580, 1398, 1377, 1343, 1234, 1231, 1194, 1146, 1127, 1119, 1068, 995, 831, 757 cm^{-1}. UV−vis (MeCN): λ_{max} (ε/M^{-1} cm^{-1}) = 429 (14 400), 338 (900), 323 (1400), 279 (20 900), 254 (17 500), 227 (19 900) nm. Emission (MeCN): λ_{em} (τ/ns) = 517 (9.4) nm.

*Synthesis of 4-(2-(2-Methoxyethoxy)ethylamino)-(N-(2-propyn-1-yl))-1,8-naphthalimide (**L3**).* This was synthesized as for **L2** using **L1** (150 mg, 0.56 mmol) and 2-(2-methoxyethoxy)ethanamine (265 mg, 2.23 mmol) to afford **L3** as a yellow solid. Yield: 94 mg, 0.27 mmol, 48.2%. ^{1}H NMR (400 MHz, $CDCl_3$): δ_H = 8.64 (d, 1H, $^{3}J_{HH}$ = 8.4 Hz), 8.50 (d, 1H, $^{3}J_{HH}$ = 8.4 Hz), 8.21 (d, 1H, $^{3}J_{HH}$ = 8.4 Hz), 7.64 (app t, 1H, $^{3}J_{HH}$ = 7.2 Hz), 6.71 (d, 1H, $^{3}J_{HH}$ = 8.5 Hz), 6.02−5.96 (broad t, 1H, N*H*), 4.95 (d, 2H, $^{4}J_{HH}$ = 2.5 Hz, CH_2), 3.91 (t, 2H, $^{3}J_{HH}$ = 5.4 Hz), 3.77−3.73 (m, 2H), 3.64−3.60 (m, 2H), 3.60 (app q, 2H, $^{3}J_{HH}$ = 4.8 Hz, CH_2), 3.44 (s, 3H, CH_3), 2.10 (t, 1H, $^{4}J_{HH}$ = 2.4 Hz, C≡C*H*) ppm. HRMS (ES+) found m/z 353.1499; $[C_{20}H_{20}N_2O_4$ + H$]^+$ requires 353.1496. IR (solid): υ = 3279, 2893, 2372, 1682, 1647, 1587, 1549, 1456, 1402, 1373, 1337, 1296, 1246, 1192, 1169, 1143, 1093, 995, 947, 837, 778 cm^{-1}. UV−vis (MeCN): λ_{max} (ε/M^{-1} cm^{-1}) = 430 (12 400), 339 (1300), 324 (1600), 279 (16 400), 254 (13 600), 227 (16 600) nm. Emission (MeCN): λ_{em} (τ/ns) = 518 (10.4) nm.

*Synthesis of 4-Piperidinyl-(N-(2-propyn-1-yl))-1,8-naphthalimide (**L4**).*[38] This was synthesized as for **L2** using **L1** (170 mg, 0.63 mmol) and piperidine (0.25 mL, 2.52 mmol) to afford **L4** as an orange solid. Yield: 133 mg, 0.42 mmol, 66.0%. ^{1}H NMR (400 MHz, $CDCl_3$): δ_H = 8.59 (d, 1H, $^{3}J_{HH}$ = 7.3 Hz), 8.52 (d, 1H, $^{3}J_{HH}$ = 8.1 Hz), 8.39 (d, 1H, $^{3}J_{HH}$ = 8.4 Hz), 7.67 (app t, 1H, $^{3}J_{HH}$ = 7.9 Hz), 7.16 (d, 1H, $^{3}J_{HH}$ = 8.1 Hz), 4.94 (d, 2H, $^{4}J_{HH}$ = 2.3 Hz), 3.4−3.2 (broad m, 4H), 2.16 (t, 1H, $^{4}J_{HH}$ = 2.3 Hz, C≡C*H*), 1.88 (app t, 4H, $^{3}J_{HH}$ = 4.9 Hz), 1.72 (app d, 2H, $^{3}J_{HH}$ = 4.8 Hz). LRMS (ES+) found m/z 319.2, $[M + H]^+$ and 382.2 $[M + H + MeCN]^+$. UV−vis (MeCN): λ_{max} (ε/M^{-1} cm^{-1}) = 410 (11 100), 340 (2400), 324 (2100), 275 (11 300), 255 (12 900), 224 (26 800), 208 (30 100) nm. Emission (MeCN): λ_{em} (τ/ns) = 535 (0.7) nm.

*Synthesis of 4-Morpholinyl-(N-(2-propyn-1-yl))-1,8-naphthalimide (**L5**).*[39] This was synthesized as for **L2** using **L1** (180 mg, 0.67 mmol) and morpholine (0.23 mL, 2.67 mmol) to afford **L5** as a bright yellow solid. Yield: 178 mg, 0.56 mmol, 83.2%. ^{1}H NMR (400 MHz, $CDCl_3$): δ_H = 8.63 (d, 1H, $^{3}J_{HH}$ = 7.3 Hz), 8.58 (d, 1H, $^{3}J_{HH}$ = 8.0 Hz), 8.40 (d, 1H, $^{3}J_{HH}$ = 8.4 Hz), 7.73 (app t, 1H, $^{3}J_{HH}$ = 7.7 Hz), 7.24 (d, 1H, $^{3}J_{HH}$ = 9.7 Hz), 4.95 (d, 2H, $^{4}J_{HH}$ = 1.9 Hz), 4.02 (t, 4H, $^{3}J_{HH}$ = 4.4 Hz), 3.27 (t, 4H, $^{3}J_{HH}$ = 4.5 Hz), 2.17 (t, 1H, $^{4}J_{HH}$ = 1.8 Hz, C≡C*H*) ppm. UV−vis (MeCN): λ_{max} (ε/M^{-1} cm^{-1}) = 396 (8300), 340 (2500), 325 (1600), 271(s) (7300), 252 (10 600), 222(s) (19 600), 208 (24 200) nm. Emission (MeCN): λ_{em} (τ/ns) = 526 (3.8) nm.

*Synthesis of 4-(4-Methylpiperidinyl-(N-(2-propyn-1-yl)))-1,8-naphthalimide (**L6**).* This was synthesized as for **L2** using **L1** (169 mg, 0.63 mmol) and 4-methylpiperidine (0.30 mL, 2.51 mmol) to afford **L6** as an orange solid. Yield: 178 mg, 0.53 mmol, 84.0%. ^{1}H NMR (400 MHz, $CDCl_3$): δ_H = 8.60 (d, 1H, $^{3}J_{HH}$ = 7.2 Hz), 8.52 (d, 1H, $^{3}J_{HH}$ = 8.1 Hz), 8.39 (d, 1H, $^{3}J_{HH}$ = 8.4 Hz), 7.67 (app t, 1H, $^{3}J_{HH}$ = 8.0 Hz), 7.18 (d, 1H, $^{3}J_{HH}$ = 8.1 Hz), 4.94 (d, 2H, $^{4}J_{HH}$ = 2.1 Hz), 3.58 (broad d, 2H, $^{3}J_{HH}$ = 12.2 Hz), 2.91 (app broad t, 2H, $^{3}J_{HH}$ = 11.8 Hz), 2.16 (t, 1H, $^{4}J_{HH}$ = 2.3 Hz, C≡C*H*), 1.86 (broad d, 2H, $^{3}J_{HH}$ = 11.2 Hz), 1.60−1.56 (m, 3H), 1.07 (d, 3H, $^{3}J_{HH}$ = 6.0 Hz) ppm. HRMS (ES+) found m/z 333.1599; $[C_{21}H_{20}N_2O_2$ + H$]^+$ requires 333.1603. IR (solid): υ = 3267, 2920, 2806, 1689, 1644, 1584, 1569, 1514, 1456, 1436, 1410, 1393, 1316, 1214, 1179, 1132, 1010, 951, 840 cm^{-1}. UV−vis (MeCN): λ_{max} (ε/M^{-1} cm^{-1}) = 410 (9000), 340 (1800), 325 (1600), 275 (8600), 255 (10 000) nm. Emission (MeCN): λ_{em} (τ/ns) = 531 (0.6, 3.7) nm.

*Synthesis of 4-(4-Ethylene ketal piperidinyl-(N-(2-propyn-1-yl)))-1,8-naphthalimide (**L7**).* This was synthesized as for **L2** using **L1** (181 mg, 0.67 mmol) and 4-piperidone ethylene ketal (0.34 mL, 2.68 mmol) to afford **L7** as a bright yellow solid. Yield: 190 mg, 0.51 mmol, 75.3%. ^{1}H NMR (400 MHz, $CDCl_3$): δ_H = 8.62 (d, 1H, $^{3}J_{HH}$ = 7.2 Hz), 8.53 (d, 1H, $^{3}J_{HH}$ = 8.1 Hz), 8.40 (d, 1H, $^{3}J_{HH}$ = 8.4 Hz), 7.71 (app t, 1H, $^{3}J_{HH}$ = 8.1 Hz), 7.21 (d, 1H, $^{3}J_{HH}$ = 8.1 Hz), 4.94 (d, 2H, $^{4}J_{HH}$ = 2.4 Hz), 4.04 (s, 4H), 3.37 (t, 4H, $^{3}J_{HH}$ = 5.9 Hz), 2.17 (t, 1H, $^{4}J_{HH}$ = 2.3 Hz, C≡C*H*), 2.03 (t, 4H, $^{3}J_{HH}$ = 5.5 Hz) ppm. HRMS (ES +) found m/z 377.1496; $[C_{22}H_{20}N_2O_4$ + H$]^+$ requires 377.1502. IR (solid): υ = 2359, 1690, 1654, 1588, 1557, 1471, 1458, 1382, 1360, 1340, 1316, 1231, 1105, 1073, 1029, 945, 932, 781, 757 cm^{-1}. UV−vis (MeCN): λ_{max} (ε/M^{-1} cm^{-1}) = 403 (9700), 340 (2300), 325 (1800), 273 (11 800), 255 (13 100) nm. Emission (MeCN): λ_{em} (τ/ns) = 524 (2.3, 3.5) nm.

DOI: 10.1021/acs.inorgchem.5b00954
Inorg. Chem. 2015, 54, 6606−6615

Complex Synthesis. *Synthesis of [Au(L1)(PPh$_3$)].* **L1** (18.2 mg, 67.5 μmol), [AuCl(PPh$_3$)] (37.1 mg, 75.0 μmol), and KO^{t}Bu (15.0 mg, 0.14 mmol) were stirred in EtOH (2 mL) in a foil-covered round-bottomed flask, under a nitrogen atmosphere for 24 h at room temperature. Two equivalents of KO^{t}Bu (15.0 mg, 0.14 mmol) was then added to the reaction mixture with stirring for a further 24 h. The ethanol was then reduced in volume and the residue dissolved in minimal $CHCl_3$. Precipitation was induced with the addition of Et_2O allowing subsequent filtration and drying to afford [Au(**L1**)(PPh$_3$)] as an off-white solid. Yield: 47.5 mg, 65.2 μmol, 96.7%. ^{1}H NMR (400 MHz, $CDCl_3$): δ_H = 8.69 (d, 1H, $^3J_{HH}$ = 7.3 Hz), 8.58 (d, 1H, $^3J_{HH}$ = 8.5 Hz), 8.53 (d, 1H, $^3J_{HH}$ = 7.9 Hz), 7.85−7.78 (m, 2H), 7.53−7.30 (m, 15H), 5.10 (s, 2H, CH_2) ppm. ^{31}P{^{1}H} NMR (121 MHz, $CDCl_3$): δ_P = +41.9 ppm. HRMS (ES+) found *m*/*z* 728.0814; [$C_{33}H_{22}AuClNO_2P$ + H]$^+$, requires 728.0821. IR (solid): υ = 1744, 1632, 1667, 1587, 1479, 1433, 1329, 1234, 1099, 1049, 989, 779 cm^{-1}. UV−vis (MeCN): λ_{max} (ε/M^{-1} cm^{-1}) = 353 (7600), 338 (8900), 322 (6600), 277 (7200) nm.

Synthesis of [Au(L2)(PPh$_3$)]. This was synthesized as for [Au(**L1**)(PPh$_3$)], but using **L2** (28.8 mg, 85.1 μmol), [AuCl(PPh$_3$)] (46.3 mg, 93.6 μmol), and KO^{t}Bu (36.0 mg, 0.36 mmol) to afford [Au(**L2**)(PPh$_3$)] as an orange solid. Yield: 55.8 mg, 70.0 μmol, 82.3%. ^{1}H NMR (400 MHz, $CDCl_3$): δ_H = 8.39 (d, 1H, $^3J_{HH}$ = 7.3 Hz), 8.33 (d, 1H, $^3J_{HH}$ = 8.4 Hz), 8.21 (d, 1H, $^3J_{HH}$ = 8.4 Hz), 7.56−7.32 (m, 15H), 6.96 (app t, 1H, $^3J_{HH}$ = 8.1 Hz), 6.56 (d, 1H, $^3J_{HH}$ = 8.4 Hz), 5.99 (t, 1H, $^3J_{HH}$ = 4.7 Hz), 5.07 (s, 2H, CH_2), 3.92 (t, 2H, $^3J_{HH}$ = 5.1 Hz), 3.89 (broad t, 2H), 3.62−3.56 (m, 2H), 3.56 (app q, 2H, $^3J_{HH}$ = 4.8 Hz), 2.36 (broad s, 1H, O*H*) ppm. ^{31}P{^{1}H} NMR (121 MHz, $CDCl_3$): δ_P = +42.6 ppm. HRMS (ES+) found *m*/*z* 797.1835; [$C_{37}H_{32}AuN_2O_4P$ + H]$^+$ requires 797.1838. IR (solid): υ = 3300, 2877, 2359, 2029, 1736, 1683, 1627, 1610, 1572, 1437, 1364, 1323, 1296, 1230, 1099, 1045, 1001, 966, 744 cm^{-1}. UV−vis (MeCN): λ_{max} (ε/M^{-1} cm^{-1}) = 429 (5400), 340 (700), 323 (1100), 275 (11 400), 260 (11 600) nm.

Synthesis of [Au(L3)(PPh$_3$)]. This was synthesized as for [Au(**L1**)(PPh$_3$)], but using **L3** (26.9 mg, 76.3 μmol), [AuCl(PPh$_3$)] (41.5 mg, 84.0 μmol), and KO^{t}Bu (32.0 mg, 0.31 mmol) to afford [Au(**L3**)(PPh$_3$)] as an orange solid. Yield: 62.0 mg, 76.4 μmol, 100.0%. ^{1}H NMR (400 MHz, $CDCl_3$): δ_H = 8.53 (d, 1H, $^3J_{HH}$ = 7.2 Hz), 8.42 (d, 1H, $^3J_{HH}$ = 8.4 Hz), 8.12 (d, 1H, $^3J_{HH}$ = 8.5 Hz), 7.53 (app t, 1H, $^3J_{HH}$ = 7.4 Hz), 7.49−7.33 (m, 15H), 6.63 (d, 1H, $^3J_{HH}$ = 8.4 Hz), 5.04 (s, 2H), 3.86 (t, 2H, $^3J_{HH}$ = 4.9 Hz, CH_2), 3.69 (t, 2H, $^3J_{HH}$ = 4.1 Hz, CH_2), 3.58−3.44 (m, 4H), 3.38 (s, 3H, CH_3) ppm. ^{31}P{^{1}H} NMR (121 MHz, $CDCl_3$): δ_P = +42.1 ppm. HRMS (ES+) found *m*/*z* 811.1993; [$C_{38}H_{34}AuN_2O_4P$ + H]$^+$ requires 811.2000. IR (solid): υ = 2918, 2858, 2164, 2019, 1969, 1629, 1579, 1537, 1470, 1433, 1393, 1373, 1337, 1246, 1198, 1146, 1096, 831, 756 cm^{-1}. UV−vis (MeCN): λ_{max} (ε/M^{-1} cm^{-1}) = 428 (8700), 339 (900), 324 (1300), 276 (16 500), 258 (17 100) nm.

Synthesis of [Au(L4)(PPh$_3$)]. This was synthesized as for [Au(**L1**)(PPh$_3$)], but using **L4** (30.8 mg, 96.7 μmol), [AuCl(PPh$_3$)] (52.7 mg, 0.11 mmol), and KO^{t}Bu (12.0 mg, 0.11 mmol) to afford [Au(**L4**)(PPh$_3$)] as a yellow solid. Yield: 33.9 mg, 43.6 μmol, 45.0%. ^{1}H NMR (400 MHz, $CDCl_3$): δ_H = 8.59 (d, 1H, $^3J_{HH}$ = 7.2 Hz), 8.51 (d, 1H, $^3J_{HH}$ = 8.1 Hz), 8.36 (d, 1H, $^3J_{HH}$ = 8.4 Hz), 7.64 (app t, 1H, $^3J_{HH}$ = 7.3 Hz), 7.56−7.34 (m, 15H), 7.14 (d, 1H, $^3J_{HH}$ = 8.1 Hz), 5.09 (s, 2H), 3.26−3.11 (broad t, 4H), 1.91−1.81 (broad m, 4H), 1.66−1.76 (broad quin, 2H) ppm. ^{31}P{^{1}H} NMR (121 MHz, $CDCl_3$): δ_P = +41.2 ppm. HRMS (ES+) found *m*/*z* 777.1938; [$C_{38}H_{32}AuN_2O_2P$ + H]$^+$ requires 777.1945. IR (solid): υ = 2927, 1740, 1689, 1655, 1583, 1477, 1435, 1377, 1316, 1246, 1233, 1177, 1155, 1099, 1128, 1074, 941, 755, 690 cm^{-1}. UV−vis (MeCN): λ_{max} (ε/M^{-1} cm^{-1}) = 408 (8300), 340 (1400), 325 (1500), 273 (11 900), 252 (17 800) nm.

Synthesis of [Au(L5)(PPh$_3$)]. This was synthesized as for [Au(**L1**)(PPh$_3$)], but using **L5** (28.0 mg, 87.5 μmol), [AuCl(PPh$_3$)] (47.6 mg, 86.2 μmol), and KO^{t}Bu (37.0 mg, 0.36 mmol) to afford [Au(**L5**)(PPh$_3$)] as a yellow solid. Yield: 59.5 mg, 76.4 μmol, 87.4%. ^{1}H NMR (400 MHz, $CDCl_3$): δ_H = 8.62 (d, 1H, $^3J_{HH}$ = 7.3 Hz), 8.56 (d, 1H, $^3J_{HH}$ = 8.0 Hz), 8.40 (d, 1H, $^3J_{HH}$ = 7.9 Hz), 7.68 (app t, 1H, $^3J_{HH}$ = 7.9 Hz), 7.51−7.34 (m, 15H), 7.21 (d, 1H, $^3J_{HH}$ = 8.1 Hz), 5.09 (d, 2H, $^5J_{HP}$ = 1.5 Hz, NCH_2), 4.01 (t, 4H, $^3J_{HH}$ = 4.6 Hz), 3.25 (t, 4H, $^3J_{HH}$ = 4.5 Hz) ppm. ^{31}P{^{1}H} NMR (121 MHz, $CDCl_3$): δ_P = +42.6 ppm. HRMS (ES+) found *m*/*z* 1237.2237; [$C_{37}H_{30}AuN_2O_3P$ + AuPPh$_3$] requires 1237.2237. IR (solid): υ = 1842, 1822, 1736, 1688, 1645, 1576, 1512, 1435, 1379, 1244, 1234, 1174, 1112, 1095, 1008, 935, 868, 779, 702 cm^{-1}. UV−vis (MeCN): λ_{max} (ε/M^{-1} cm^{-1}) = 393 (6900), 340 (2800), 272 (13 100), 255 (16 600) nm.

Synthesis of [Au(L6)(PPh$_3$)]. This was synthesized as for [Au(**L1**)(PPh$_3$)], but using **L6** (30.5 mg, 91.8 μmol), [AuCl(PPh$_3$)] (50.0 mg, 101.0 μmol), and KO^{t}Bu (39.0 mg, 0.38 mmol) to afford [Au(**L6**)(PPh$_3$)] as an orange solid. Yield: 59.6 mg, 75.4 μmol, 82.1%. ^{1}H NMR (400 MHz, $CDCl_3$): δ_H = 8.59 (d, 1H, $^3J_{HH}$ = 7.3 Hz), 8.51 (d, 1H, $^3J_{HH}$ = 8.1 Hz), 8.35 (d, 1H, $^3J_{HH}$ = 7.9 Hz), 7.63 (app t, 1H, $^3J_{HH}$ = 7.9 Hz), 7.52−7.44 (m, 15H), 7.15 (d, 1H, $^3J_{HH}$ = 8.1 Hz), 5.09 (d, 2H, $^5J_{HP}$ = 1.6 Hz), 3.56 (app broad d, 2H, $^3J_{HH}$ = 11.8 Hz), 2.89 (broad t, 2H, $^3J_{HH}$ = 11.5 Hz), 1.85 (app broad d, 2H, $^3J_{HH}$ = 9.5 Hz), 1.62 (app broad d, 1H, $^3J_{HH}$ = 7.3 Hz), 1.58 (app s, 2H, CH_2), 1.07 (d, 3H, $^3J_{HH}$ = 5.9 Hz, CH_3) ppm. ^{31}P{^{1}H} NMR (121 MHz, $CDCl_3$): δ_P = +42.6 ppm. HRMS (ES+) found *m*/*z* 791.2092; [$C_{39}H_{34}AuN_2O_2P$ + H]$^+$ requires 791.2096. IR (solid): υ = 1734, 1688, 1647, 1583, 1516, 1481, 1456, 1435, 1412, 1377, 1336, 1244, 1226, 1174, 1153, 1130, 1076, 966, 792, 751 cm^{-1}. UV−vis (MeCN): λ_{max} (ε/M^{-1} cm^{-1}) = 407 (5300), 339 (1300), 326 (1500), 277(s) (10 900), 259 (13 500), 245 (13 300) nm.

Synthesis of [Au(L7)(PPh$_3$)]. This was synthesized as for [Au(**L1**)(PPh$_3$)], but using **L7** (34.1 mg, 90.6 μmol), [AuCl(PPh$_3$)] (49.3 mg, 99.6 μmol), and KO^{t}Bu (38.0 mg, 0.37 mmol) to afford [Au(**L7**)(PPh$_3$)] as a bright yellow solid. Yield: 70.3 mg, 84.2 μmol, 92.6%. ^{1}H NMR (400 MHz, $CDCl_3$): δ_H = 8.61 (d, 1H, $^3J_{HH}$ = 7.6 Hz), 8.53 (d, 1H, $^3J_{HH}$ = 8.4 Hz), 8.37 (d, 1H, $^3J_{HH}$ = 9.6 Hz), 7.67 (app t, 1H, $^3J_{HH}$ = 8.4 Hz), 7.52−7.37 (m, 15H), 7.20 (d, 1H, $^3J_{HH}$ = 8.0 Hz), 5.09 (d, 2H, $^5J_{HP}$ = 1.6 Hz), 4.04 (s, 4H), 3.35 (broad t, 4H, $^3J_{HH}$ = 6.0 Hz), 2.03 (broad t, 4H, $^3J_{HH}$ = 6.0 Hz) ppm. ^{31}P{^{1}H} NMR (121 MHz, $CDCl_3$): δ_P = +42.1 ppm. HRMS (ES+) found *m*/*z* 835.1993; [$C_{40}H_{34}AuN_2O_4P$ + H]$^+$ requires 835.1994. IR (solid): υ = 2847, 1736, 1695, 1655, 1589, 1481, 1462, 1437, 1411, 1383, 1336, 1315, 1232, 1172, 1141, 1101, 1076, 1028, 947, 914, 887, 842, 781, 753, 692 cm^{-1}. UV−vis (MeCN): λ_{max} (ε/M^{-1} cm^{-1}) = 400 (8500), 340 (1900), 325 (1600), 274(s) (12 700), 254 (18 000) nm.

RESULTS AND DISCUSSION

Synthesis and Characterization. The ligands (**L1**−**L7**) were synthesized from 4-chloro-1,8-naphthalic anhydride in a one- (**L1**) or two-step process (Scheme 1). First, reaction with propargyl amine in ethanol yielded the corresponding 4-chloro-1,8-naphthalimide species, **L1**. Further functionalization of this pro-ligand, allowing the tuning of physical and electronic properties, was achieved by heating **L1** with a selection of different amines in DMSO to yield **L2**−**L7**. The seven ligands were characterized by ^{1}H NMR spectroscopy (e.g., Supporting Information Figure S1) and high-resolution mass spectrometry (HRMS) studies. Interestingly, the methylene group adjacent to the alkyne (δ_H ca. 4.95 ppm) showed a $^4J_{HH}$ of ca. 2.5 Hz caused by coupling to the terminal alkyne proton. Each of the ligands was then reacted with [AuCl(PPh$_3$)] in EtOH, in the presence of KO^{t}Bu, to generate the corresponding Au(I) complexes as air-stable, light-sensitive yellow powders (Scheme 1). An excess of base, added in two aliquots over a period of 48 h, was generally required for the reaction to proceed to completion.

In addition to the solution-state characterization, two single crystal structural determinations (Figure 1) were obtained for **L6** and the corresponding complex, **Au-L6**. For **L6**, crystals were grown from the slow evaporation of a chloroform/hexane solution; for **Au-L6**, crystals were obtained from slow evaporation of a chloroform/acetonitrile solution of the

DOI: 10.1021/acs.inorgchem.5b00954
Inorg. Chem. 2015, 54, 6606−6615

Scheme 1. Synthetic Route to the Ligands and Au(I) Complexes[a]

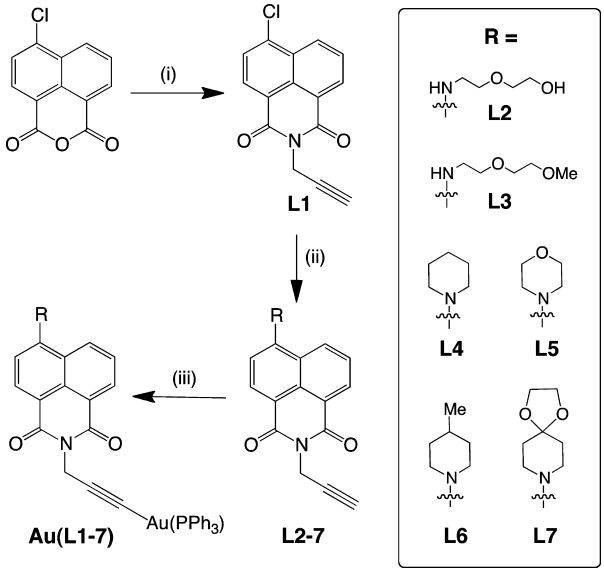

[a](i) Propargyl amine, EtOH, heat; (ii) amine, DMSO, heat; (iii) [AuCl(PPh$_3$)], EtOH, KO^{t}Bu.

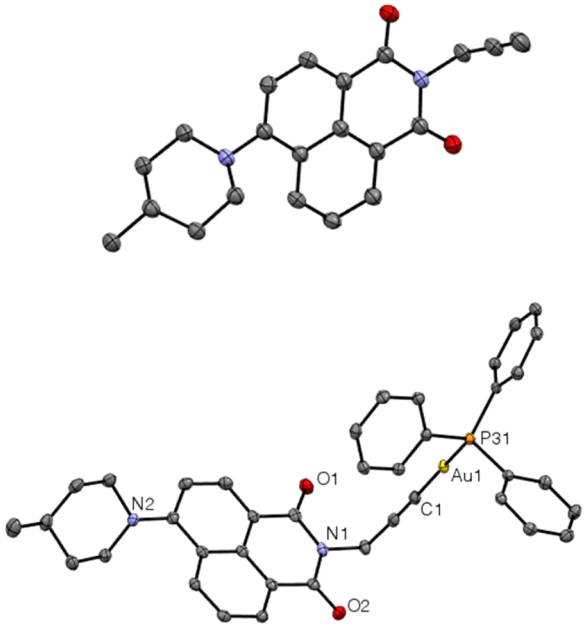

Figure 1. X-ray crystal structure of **L6** (top) and **Au-L6** (bottom) with ellipsoids at 50% occupancy. Hydrogen atoms omitted for clarity.

complex. The data collection parameters are in the Supporting Information (Table S1). The structure of the ligand shows the anticipated configuration with the piperidine unit twisted out of the plane of the naphthalimide unit. For the complex, the structure shows the expected two-coordinated Au(I) center with d(Au−C) and d(Au−P) at 1.995(3) and 2.2758(7) Å, respectively.[40] There is a notable deviation from ideal linearity across the four-center alkyne-gold-phosphine (C≡C−Au−P) moiety, with corresponding bond angles of 169.80(7)° and 167.7(2)° for angles C(1)−Au(1)−P(31) and C(2)−C(1)−Au(1), respectively. In the crystal the complex packs in a tail-to-tail arrangement (Supporting Information Figure S2) that allows neighboring naphthalimide units to interact through intermolecular $\pi-\pi$ distances of approximately 3.34−3.57 Å.

The complexes were also fully characterized using multinuclear NMR spectroscopy, HRMS, and IR studies. ^{31}P{^{1}H} NMR was particularly useful in confirming the coordination of the alkyne moiety to the Au(I) center, which induced an ca. +12 ppm shift (relative to [AuCl(PPh$_3$)]) of the single phosphine resonance to around +42 ppm, consistent with related reports on two-coordinate Au(I) species involving alkyne/phosphine donors.[41] The disappearance of the alkyne signal in the ^{1}H NMR spectra, and the induced shift of the methylene resonance to ca. 5.1 ppm (e.g., Supporting Information Figure S1), provided further confirmation of C−Au bond formation. This latter signal was split into a doublet, apparently attributed to a $^5J_{HP}$ coupling of ca. 1.5 Hz, providing categorical evidence of the proposed binding mode.

The solution absorption spectra of **L1**−**7** (Table 1), with the exception of **L1**, were composed of at least two dominant

Table 1. UV−Vis Absorption and Emission Properties of the Ligands (in Parentheses) and Complexes

complex	λ_{max}/nm[a]	λ_{em}/nm[a,b]	τ/ns[a,c]	Φ[d]
Au-L1	353 (353)	391 (392)	−[e] (3.0)	<0.01
Au-L2	429 (429)	514 (517)	10.1 (9.4)	0.50
Au-L3	428 (430)	515 (518)	10.0 (10.4)	0.60
Au-L4	408 (410)	532 (535)	1.2 (0.7)	0.06
Au-L5	393 (396)	523 (526)	5.7 (3.8)	0.60
Au-L6	407 (410)	530 (531)	1.2, 2.6 (0.6, 3.7)	0.11
Au-L7	400 (403)	521 (524)	4.7 (2.3, 3.5)	0.22

[a]10^{-5} M MeCN. [b]λ_{ex} = 415 nm. [c]λ_{ex} = 295 or 372 nm. [d]In aerated MeCN. [e]Too weak.

absorptions: two sets of structured $\pi-\pi^*$ transitions between 300 and 240 nm and a broad band centered at 400−430 nm attributed to intramolecular charge transfer (ICT) character (arising from the electron-donating character of the amino substituent and the electron-accepting ability of the naphthalimide core). The variable electron-donating character of the 4-amino groups modulated the absorption energy of the ICT band. This is a crucial consideration for applications such as cell imaging in that subtle changes in the structure of the amine substituent can induce a shift in the position of the ICT band. For **L2** and **L3**, this resulted in the most bathochromically shifted ICT absorption, which also correlated with the greatest upfield shift of the aromatic proton at the 3-position (i.e., adjacent to the amine substituent). **L1** displayed significantly different UV absorption properties, notably the lack of the ICT band and a large red-shift of the $\pi-\pi^*$ bands. For the complexes, Table 1 clearly demonstrates that the absorption properties are dominated by ligand character and, in particular, the ICT-based transition, with associated molar absorption coefficients of >5 × 10^3 M^{-1} cm^{-1}.

Solutions of **L2**−**7** were also found to be highly fluorescent (see Experimental Section). When using an excitation wavelength of 385−430 nm on aerated MeCN solutions of the ligands, a visible emission band at ca. 520 nm was observed (Supporting Information Figure S3). The advantageous Stokes' shifts were greatest for the piperidine and morpholine substituted ligands/complexes (up to 6500 cm^{-1}) and consistent with an excited state dominated by ICT character. It is notable that very subtle changes in the substituted amine (e.g., **L4** versus **L5**) induced measurable changes in emission

DOI: 10.1021/acs.inorgchem.5b00954
Inorg. Chem. 2015, 54, 6606−6615

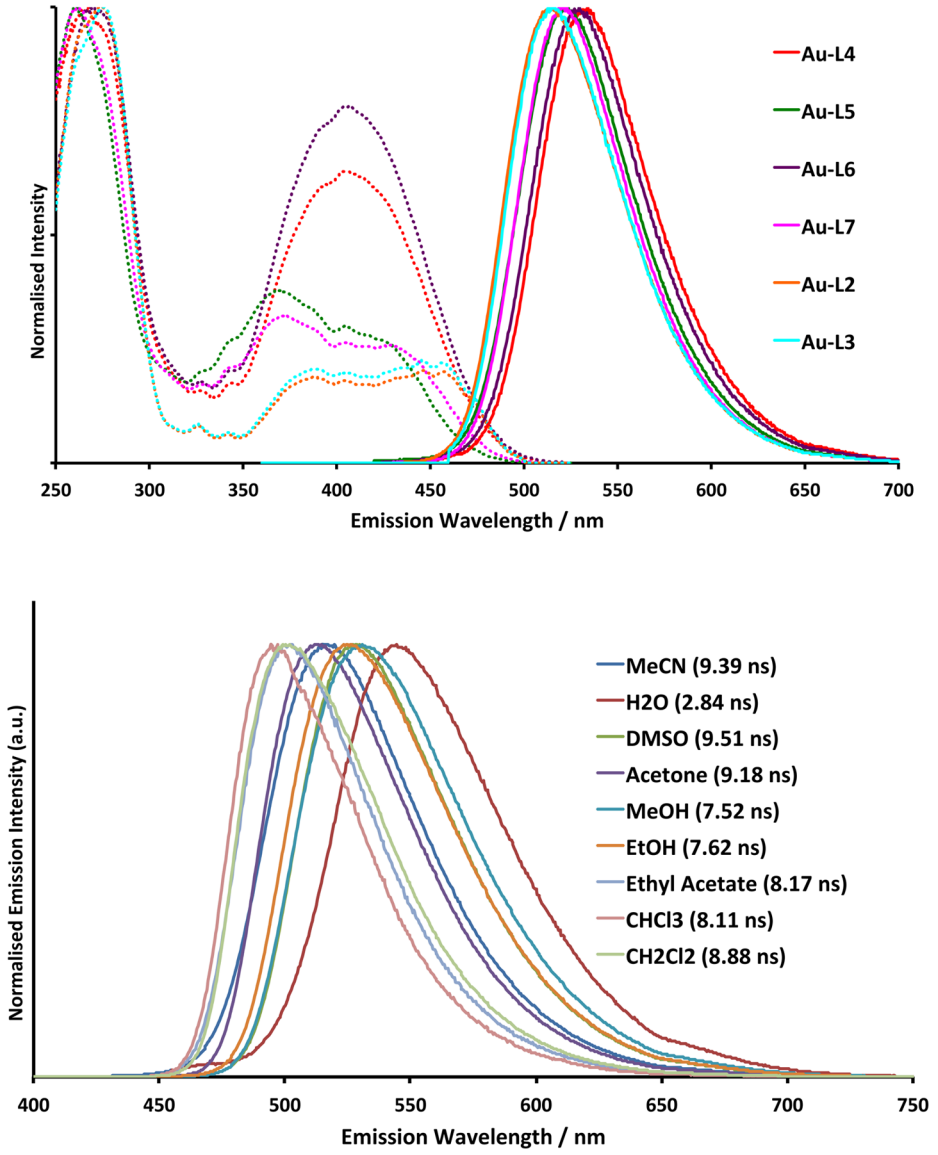

Figure 2. Top: Excitation (dashed) and emission (solid) profiles for selected complexes (recorded in MeCN using λ_{exc} = 415 nm, λ_{em} = 535 nm). Bottom: Emission data for **L2** in different solvents (λ_{exc} = 415 nm) with corresponding lifetimes (λ_{exc} = 372 nm) in parentheses.

maxima. Supporting time-resolved measurements revealed lifetimes (<11 ns) that were indicative of fluorescence. These observations are also consistent with our previous work on this class of chromophore[42] and that by others,[43] showing that the ICT fluorescent character is imparted by the presence of a donor group at the naphthalimide core.

Further studies on the solvent dependence of the emission properties were investigated using the most hydrophilic derivative, **L2**, which facilitated comparative studies across a range of solvents, including water. Both steady-state and lifetime measurements were obtained in a range of solvents (ethyl acetate, dichloromethane, chloroform, acetone, ethanol, methanol, dimethyl sulfoxide, water) of varying polarity. The results show a highly solvent-dependent 50 nm shift in emission maximum across the solvent range (Figure 2), with the most polar solvent inducing the largest bathochromic shift of the fluorescence, thus indicating a positive solvatochromism associated with the ICT state. The lifetimes also show considerable variation across the solvent range (2.8 ns in water versus 8.2 ns in ethyl acetate) and suggest that such chromophores may be applicable to fluorescence lifetime imaging microscopy (FLIM) when regarding localization in lipo- versus hydrophilic cellular compartments. It is also important to note that **L2** retained its advantageous fluorescence properties in aqueous solution, suggesting good compatibility with biological environments and amenability with further confocal microscopy studies. Overall it appears that photoinduced electron transfer, which can account for significant quenching in amino-substituted naphthalimide chromophores, is not problematic in these systems. Upon coordination to Au(I), each of the ligands retained their characteristic luminescence properties[44] (Table 1) with a slight hypsochromic shift for the emission maxima. Relative to the free ligands fluorescence lifetimes were generally extended for the complexes, while the quantum yields were wide-ranging in aerated solution, but up to ca. 60% for the most emissive examples. The data suggest that a bathochromic shift in λ_{em} was generally accompanied by a significant reduction in quantum yield and lifetime.

DOI: 10.1021/acs.inorgchem.5b00954
Inorg. Chem. 2015, 54, 6606−6615

Table 2. Cytotoxicity IC_{50} (μM) Values of the Ligands and Complexes[a]

	LOVO	A549	PC3	MCF7	HEK
Au-L1	>100	>100	>100	>100	8.02 (1.03)
L1	76.21 (8.36)	>100	>100	>100	22.68 (7.51)
Au-L2	5.88 (0.72)	41.84 (6.57)	6.76 (0.88)	6.85 (0.75)	4.41 (0.55)
L2	57.56 (1.91)	>100	>100	66.16 (1.19)	35.25 (1.52)
Au-L3	5.12 (0.62)	51.96 (5.77)	8.26 (1.07)	6.23 (0.55)	0.77 (0.07)
L3	>100	>100	>100	>100	28.42 (6.95)
Au-L4	39.73 (5.92)	>100	45.35 (12.19)	59.02 (1.64)	6.65 (1.04)
L4	>100	>100	>100	>100	7.11 (1.75)
Au-L5	10.32 (1.00)	>100	39.86 (9.58)	49.41 (8.51)	3.87 (0.77)
L5	>100	>100	>100	>100	>100
Au-L6	>100	>100	>100	68.34 (4.96)	9.53 (3.13)
L6	>100	>100	>100	>100	3.14 (0.75)
Au-L7	34.47 (5.16)	89.92 (5.72)	69.26 (4.91)	8.88 (0.14)	3.56 (0.25)
L7	>100	>100	>100	>100	6.61 (0.63)

[a]Using MTT assay; standard deviation given in parentheses.

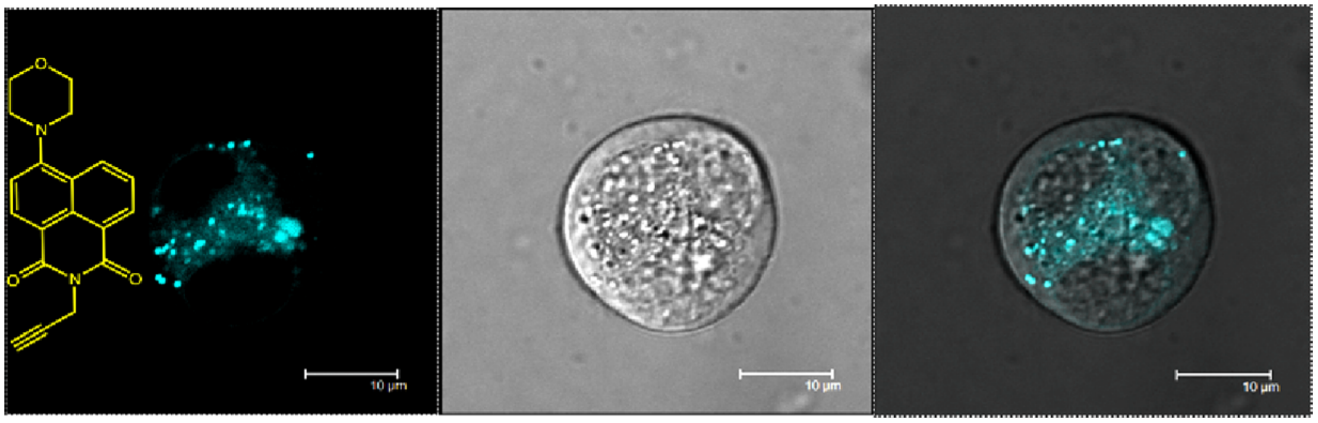

Figure 3. Microscopy of HEK cells imaged with **L5** (morpholine) using fluorescence (left; λ_{ex} = 405 nm and λ_{em} = 535 nm), transmitted light (middle), and overlay (right). Cells incubated with 100 μg mL^{-1} of the lumophore.

Confocal Fluorescence Microscopy Studies. Prior to microscopy studies, the ligands and complexes were assessed for cytotoxicity effects using the standard MTT assay against MCF7 (breast adenocarcinoma), A549 (lung adenocarcinoma), PC3 (prostate adenocarcinoma), LOVO (colon adenocarcinoma), and HEK cell lines; IC_{50} values for these compounds are shown in Table 2. The compounds were initially dissolved in DMSO, and doses of 0.1, 1, 10, and 100 μM were tested to screen the activity of different concentrations while comparing to a control medium with no treatment. First, it is clear that the Au(I) complexes were significantly more toxic than the corresponding free ligands, an observation previously noted with Au(I) complexes of alkynyl-anthraquinone ligands.[19] This also correlates with the relatively enhanced lipophilicities of the complexes (presumably via the coordinated PPh_3 ligand), which was supported by calculated partition coefficient log P_{calc} values (see below). Second, all compounds were more toxic to HEK cells than the cancer cell lines.

For the ligands, chloro-derived **L1** showed some selectivity for LOVO among the cancer cell lines, while the glycol variant **L2** was also inhibitive to MCF7. The complexes possessing the glycol appended substituted amine, **Au-L2** and **Au-L3**, appear most potent, while **Au-L6** showed some selectivity for MCF7 over the other cancer cell lines. Importantly, the stability of the Au(I) complexes in d_6-DMSO was determined using ^{31}P NMR spectroscopy, which showed (for 96 h at 37 °C) only trace levels of either Ph_3P or Ph_3PO, suggesting that ligand displacement is not problematic under such conditions and complexes remain intact.

Confocal fluorescence microscopy was performed using both HEK cells and the protistan fish parasite *Spironucleus vortens* (*S. vortens*). The fluorescent compounds used for imaging studies were added as 3−10 mM solutions in DMSO, with the final concentration on the slide reduced 10-fold. Imaging work showed that the naphthalimide chromophores were capable of providing bright fluorescence signals even in polar solvent environments, as evidenced by the spectroscopic studies. In all cases, an excitation wavelength of 405 nm was used together with a detection wavelength between 530 and 580 nm. Ligands **L2** (log P_{calc} = 1.285), **L3** (log P_{calc} = 1.807), **L5** (log P_{calc} = 2.117), and **L7** (log P_{calc} = 2.549) and their corresponding complexes **Au-L2** (log P_{calc} = 3.757), **Au-L3** (log P_{calc} = 4.280), **Au-L5** (log P_{calc} = 4.590), and **Au-L7** (log P_{calc} = 5.022), which possess structural variance and increasing lipophilicities across the range, were selected for imaging studies.

In general, uptake into HEK cells was slow, and in a number of cases insufficient to allow quality images to be obtained. The morpholine derivative, **L5**, gave the brightest images with clear staining of both the plasma and the nuclear membranes, including some background nuclear fluorescence. **L5** (Figure 3) also showed very distinct localization with high intensity punctate fluorescence suggestive of organelle staining/uptake.

DOI: 10.1021/acs.inorgchem.5b00954
Inorg. Chem. 2015, 54, 6606−6615

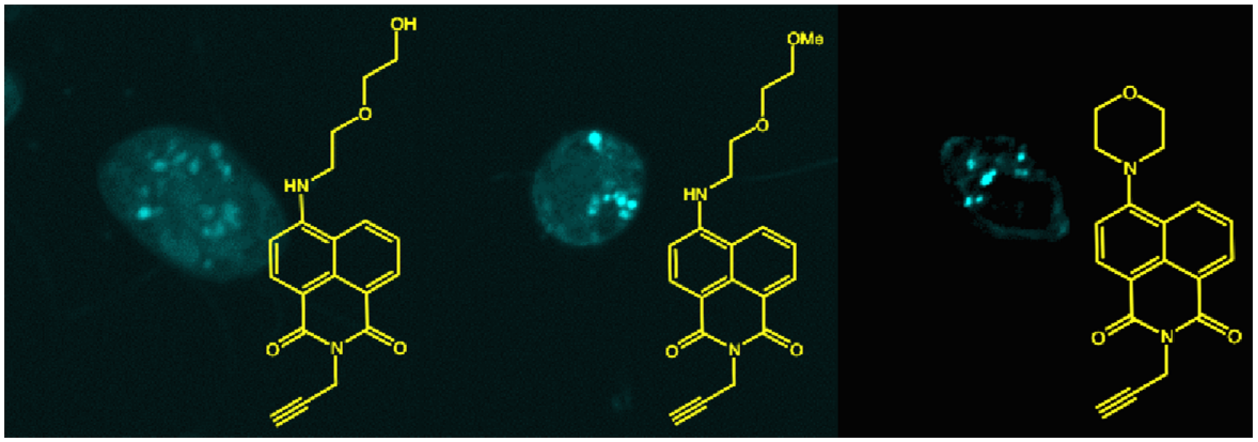

Figure 4. Fluorescence microscopy of HEK cells imaged with (left to right) **L2** (glycol), **L3** (ether), both showing relatively weak uptake and fluorescent signals, and **L5** (morpholine) showing localized signals (λ_{ex} = 405 nm and λ_{em} = 535 nm). Cells incubated with 100 μg mL^{-1} of the lumophore.

The ligands **L2**, **L3**, and **L7** showed varied uptake for the HEK cells with relatively weak fluorescent signals evident (Figure 4).

Complexes **Au-L2** and **Au-L7** showed very limited uptake, even after 30 min. Uptake into HEK cells was best demonstrated using **Au-L5**; the imaged cells showed staining of filapodia (fine protuberances from the cell surface) and various internal organelles and glycogen vacuoles (Supporting Information Figure S4). The methoxy glycol derivative, **Au-L3**, showed slow uptake, but still produced good quality images after 55 min (Figure 5). The fluorochrome was incorporated within ring shaped structures at the cell surface (possibly indicative of an apoptotic event, membrane blebs, or autophagosomes), as well as general membrane structures and lipid-rich areas. Comparative images using the commercial stain TMRE, which selectively targets mitochondria, showed excellent separation of the fluorophore signals (TMRE vs **Au-L3**) and a clear area of colocalization, suggesting **Au-L3** has some affinity for mitochondrial-rich environments. This contrasts with the biodistribution into the nuclei of MCF7 cells demonstrated by the Au(I) complexes of mercaptonaphthalimide ligands.[16]

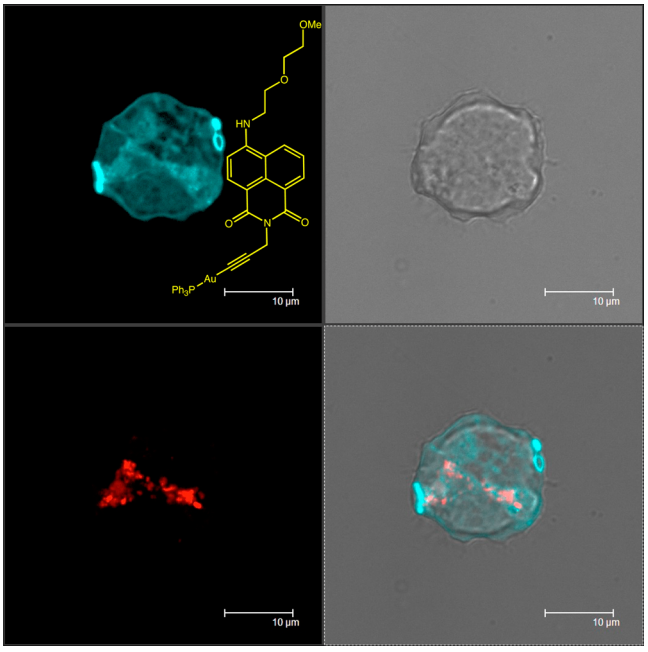

Figure 5. Microscope images of HEK cells incubated with **Au-L3** (glycol methyl ether) and TMRE showing (clockwise from top left): blue/green fluorescence from **Au-L3** (λ_{ex} = 488 nm; λ_{em} = 535 nm), transmission image, overlaid images showing some degree of colocalization, red fluorescence from TMRE (λ_{ex} = 543 nm; λ_{em} = 600 nm). Cells incubated with 100 μg mL^{-1} of the lumophore.

Imaging experiments were also undertaken with the fish parasite, *S. vortens*,[45] using the same selection of probes (Supporting Information Figures S5−S9). First, much better uptake was generally observed as compared to the HEK cell work, and no evidence of compound toxicity was witnessed throughout the duration of the studies on *S. vortens* (stable populations over a 2−3 h period). **L2** showed specific hydrogenosome (organelles related to mitochondria[46]) staining and faint nuclear fluorescence, albeit with a stronger background of cytosol staining than the other free ligands. The ketal derivative, **L7**, produced excellent images at significantly reduced (60−75%) laser power, staining the plasma and nuclear membrane, with very bright hydrogenosomes and larger lipid droplets, as well as some flagella staining (Figure 6). Last, **L5** again very specifically stained hydrogenosomes, with significantly reduced cytosol staining as compared to **L2**.

Interestingly, despite the excellent results obtained with **L5**, **Au-L5** showed very limited uptake into *S. vortens*; this observation also contrasts with the favorable uptake of **Au-L5** by HEK cells. Conversely, **Au-L7**, which showed poor uptake in HEK cells, showed excellent uptake by *S. vortens*. The images obtained with **Au-L7** showed very brightly localized spots (Supporting Information Figure S9) of fluorescence consistent with hydrogenosome staining together with labeling of larger lipid droplets. **Au-L2** again showed limited uptake, while **Au-L3** produced good quality images (Supporting Information Figure S8), which facilitated further colocalization analyses using TMRE and CTC (5-cyano-2,3-ditolyltetrazolium chloride).

The imaging results present clear evidence of the biocompatible utility of the substituted naphthalimide fluorophores toward cell imaging using confocal fluorescence microscopy. For the ligands the morpholine substituent (**L5**) imparts very favorable characteristics, enhancing uptake and enabling some distinct localization patterns. It is evident that incorporating these ligands into the gold complexes enhances

DOI: 10.1021/acs.inorgchem.5b00954
Inorg. Chem. 2015, 54, 6606−6615

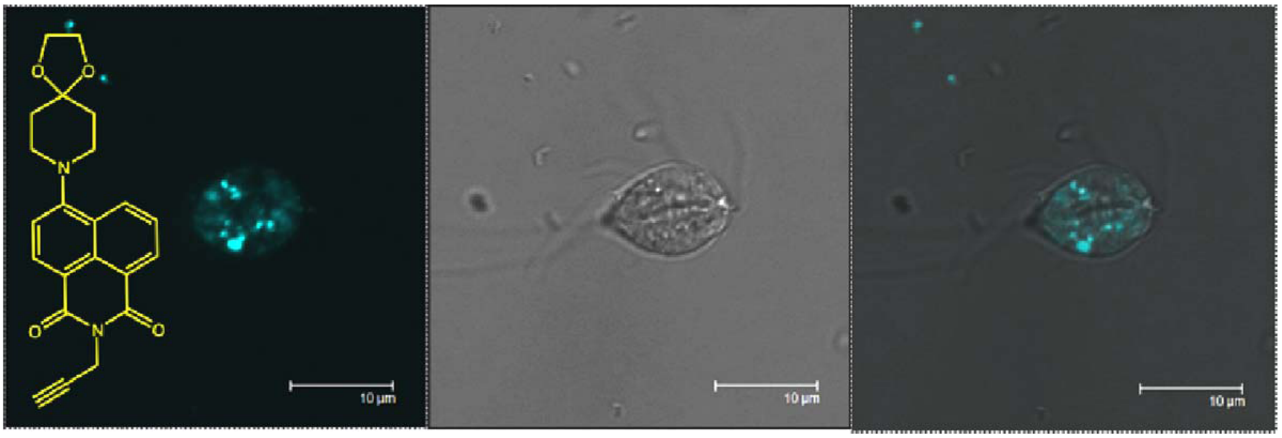

Figure 6. Microscopy of *S. vortens* imaged with **L7** using fluorescence (left; λ_{ex} = 405 nm and λ_{em} = 535 nm), transmitted light (middle), and overlay (right). Cells incubated with 100 μg mL^{-1} of the lumophore.

their lipophilicity, but also leads to very different behavior (both for imaging and for cytotoxicity). The uptake of the complexes into HEK cells seem to correlate with the predicted lipophilicities; that is, the more lipophilic species (e.g., **L5**, **Au-L5**) showed the best uptake; however, this does not seem to be the case with the *S. vortens* studies. Importantly, it appears that the specific nature of the amine substituent can be used to tune the imaging capability, specifically uptake and localization, of the probes. Very basic changes to the ligand structure (e.g., **L2** versus **L3**) can have a profound influence upon the imaging capability of a given probe.

CONCLUSIONS

This Article has described the synthetic development of an alkynyl-derived series of 1,8-naphthalimide fluorophores, generating seven ligands that can in turn be utilized for Au(I) coordination chemistry. The structural variants seek to address the balance between hydro- and lipophilic character. The optical properties of the fluorophores are dictated by ligand-centered, ICT-dominated transitions that provide visible absorption and emission characteristics, the latter often associated with lifetimes up to ca. 10 ns and quantum yields in excess of 50%. Cytotoxicity assessments revealed that all compounds were more toxic to the HEK cells than a variety of cancer cell lines, and that the Au(I) complexes were generally more toxic than the corresponding ligands. Cellular imaging studies were conducted on both HEK cells and *Spironucleus vortens* and showed the comparative imaging capabilities of selected ligands and complexes. The specific cellular uptake and localization characteristics can be controlled by the nature of the molecular structure, with starkly contrasting uptake behavior between ligand/complex pairs. Certainly, the more lipophilic fluorophores (e.g., **L5**) showed a propensity for localizing in subcellular environments such as mitochondria (HEK) and hydrogenosomes (*S. vortens*). Cellular imaging studies with emissive lanthanide complexes have also shown that the nature of a fluorophore substituent can influence their intracellular uptake, distributions, and cytotoxicity, perhaps through varied affinities for proteins.[47]

ASSOCIATED CONTENT

Supporting Information

X-ray crystallographic data for **L6** and **Au-L6** in CIF format. X-ray crystal data, examples of ^{1}H NMR, further examples of luminescence profiles, and additional confocal fluorescence images. The Supporting Information is available free of charge on the ACS Publications website at DOI: 10.1021/acs.inorgchem.5b00954.

AUTHOR INFORMATION

Corresponding Author

*E-mail: popesj@cardiff.ac.uk.

Notes

The authors declare no competing financial interest.

ACKNOWLEDGMENTS

We thank Cardiff University for support, the EPSRC UK National Crystallographic Service, University of Southampton, and the EPSRC UK National Mass Spectrometry Facility, Swansea University. Johnson Matthey PLC are thanked for the loan of hydrogen tetrachloroaurate(III).

REFERENCES

(1) (a) Higby, G. J. *Gold Bull.* **1982**, *15*, 130. (b) Sadler, P. J. *Struct. Bonding (Berlin)* **1976**, *29*, 171. (c) Shaw, C. F., III. *Chem. Rev.* **1999**, *99*, 2589.

(2) (a) Mjos, K. D.; Orvig, C. *Chem. Rev.* **2014**, *114*, 4540. (b) Kean, W. F.; Forestier, F.; Kassam, Y.; Buchanan, W. W.; Rooney, P. J. *Semin. Arthritis Rheum.* **1985**, *14*, 180.

(3) (a) Tiekink, E. R. T. *Crit. Rev. Oncol. Hematol.* **2002**, *42*, 225. (b) Lewis, A. J.; Walz, D. T. *Prog. Med. Chem.* **1982**, *19*, 1.

(4) Gunatilleke, S. S.; Barrios, A. M. *J. Med. Chem.* **2006**, *49*, 3933.

(5) (a) Stanley, B. A.; Sivakumaran, V.; Shi, S.; McDonald, I.; Lloyd, D.; Watson, W. H.; Aon, M. A.; Paolocci, N. *J. Biol. Chem.* **2011**, *286*, 33669. (b) Williams, C. F.; Yarlett, N.; Aon, M. A.; Lloyd, D. *Mol. Biochem. Parasitol.* **2014**, *196*, 45. (c) Serebryanskaya, T. V.; Lyakhov, A. S.; Ivashkevich, L. S.; Schur, J.; Frias, C.; Prokop, A.; Ott, I. *Dalton Trans.* **2015**, *44*, 1161.

(6) Messori, L.; Marcon, G. Metal Ions in Biological Systems. In *Metal Ions and Their Complexes in Medication*; Sigel, A., Sigel, H., Eds.; Marcel Dekker Inc.: New York, 2004; pp 279−304.

(7) The Research Committee of the Empire Rheumatism Council. *Ann. Rheum. Dis.* **1960**, *19*, 95.

(8) Ott, I. *Coord. Chem. Rev.* **2009**, *253*, 1670.

(9) Berners-Price, S. J.; Filipovska, A. *Metallomics* **2011**, *3*, 863.

(10) (a) Fernandez-Moreira, V.; Thorp-Greenwood, F. L.; Coogan, M. P. *Chem. Commun.* **2010**, *46*, 186. (b) Lo, K. K.-W.; Choi, A. W.-T.; Law, W. H.-T. *Dalton Trans.* **2012**, *41*, 6021. (c) Coogan, M. P.; Pope, S. J. A. Application of d- and f-block fluorescent cell imaging agents. In

DOI: 10.1021/acs.inorgchem.5b00954
Inorg. Chem. 2015, 54, 6606−6615

The Chemistry of Molecular Imaging; Long, N. J.; Wong, W.-T., Eds.; Wiley: NJ, 2015; pp 275−296.
(11) For example: Baggaley, E.; Gill, M. R.; Green, N. H.; Turton, D.; Sazanovich, I. V.; Botchway, S. W.; Smythe, C.; Haycock, J. W.; Weinstein, J. A.; Thomas, J. A. *Angew. Chem., Int. Ed.* **2014**, *53*, 3367.
(12) For example: Balasingham, R. G.; Thorp-Greenwood, F. L.; Williams, C. F.; Coogan, M. P.; Pope, S. J. A. *Inorg. Chem.* **2012**, *51*, 1419.
(13) For example: Li, C.; Yu, M.; Sun, Y.; Yongquan, W.; Huang, C.; Li, F. *J. Am. Chem. Soc.* **2011**, *133*, 11231.
(14) For example: Botchway, S. W.; Charnley, M.; Haycock, J. W.; Parker, A. W.; Rochester, D. L.; Weinstein, J. A.; Williams, J. A. G. *Proc. Natl. Acad. Sci. U.S.A.* **2008**, *105*, 16071.
(15) Bagowski, C. P.; You, Y.; Scheffler, H.; Vlecken, D. H.; Schmitz, D. J.; Ott, I. *Dalton Trans.* **2009**, 10799.
(16) Ott, I.; Xu, Y.; Qian, X. *J. Photochem. Photobiol., B* **2011**, *105*, 75.
(17) Barnard, P. J.; Wedlock, L. E.; Baker, M. V.; Berners-Price, S. J.; Joyce, D. A.; Skelton, B. W.; Steer, J. H. *Angew. Chem., Int. Ed.* **2006**, *45*, 5966.
(18) Meyer, A.; Bagowski, C. P.; Kokoschka, M.; Stefanopoulou, M.; Alborzinia, H.; Can, S.; Vlecken, D. H.; Sheldrick, W. S.; Wolfl, S.; Ott, I. *Angew. Chem., Int. Ed.* **2012**, *51*, 8895.
(19) Balasingham, R. G.; Williams, C. F.; Mottram, H. J.; Coogan, M. P.; Pope, S. J. A. *Organometallics* **2012**, *31*, 5835.
(20) Langdon-Jones, E. E.; Pope, S. J. A. *Chem. Commun.* **2014**, *50*, 10343.
(21) Citta, A.; Schuh, E.; Mohr, F.; Folda, A.; Massimino, M. L.; Bindoli, A.; Casini, A.; Rigobello, M. P. *Metallomics* **2013**, *5*, 1006.
(22) Bertrand, B.; de Almeida, A.; van der Burgt, E. P. M.; Picquet, M.; Citta, A.; Folda, A.; Rigobello, M. P.; Le Gendre, P.; Bodio, E.; Casini, A. *Eur. J. Inorg. Chem.* **2014**, 4523.
(23) Arcau, J.; Andermark, V.; Aguilo, E.; Gandioso, A.; Moro, A.; Cetina, M.; Lima, J. C.; Rissanen, K.; Ott, I.; Rodriguez, L. *Dalton Trans.* **2014**, *43*, 4426.
(24) Fernandez-Moreira, V.; Marzo, I.; Gimeno, M. C. *Chem. Sci.* **2014**, *5*, 4434.
(25) (a) Gunnlaugsson, T.; Glynn, M.; Tocci, G. M.; Kruger, P. E.; Pfeffer, F. M. *Coord. Chem. Rev.* **2006**, *250*, 3094. (b) Banerjee, S.; Kitchen, J. A.; Gunnlaugsson, T.; Kelly, J. M. *Org. Biomol. Chem.* **2013**, *11*, 5642.
(26) (a) Banerjee, S.; Veale, E. B.; Phelan, C. M.; Murphy, S. A.; Tocci, G. M.; Gillespie, L. J.; Frimannsson, D. O.; Kelly, J. M.; Gunnlaugsson, T. *Chem. Soc. Rev.* **2013**, *42*, 1601. (b) Ott, I.; Xu, Y.; Liu, J.; Kokoschka, M.; Harlos, M.; Sheldrick, W. S.; Qian, X. *Bioorg. Med. Chem.* **2008**, *16*, 7107.
(27) For example: (a) Srikun, D.; Miller, E. W.; Domaille, D. W.; Chang, C. J. *J. Am. Chem. Soc.* **2008**, *130*, 4596. (b) Zhu, B.; Zhang, X.; Li, Y.; Wang, P.; Zhang, H.; Zhuang, X. *Chem. Commun.* **2010**, *46*, 5710. (c) Wang, Q.; Li, C.; Zou, Y.; Wang, H.; Yi, T.; Huang, C. *Org. Biomol. Chem.* **2012**, *10*, 6740. (d) Lee, M. H.; Han, J. H.; Kwon, P.-S.; Bhuniya, S.; Kim, J. Y.; Sessler, J. L.; Kang, C.; Kim, J.-S. *J. Am. Chem. Soc.* **2012**, *134*, 1316.
(28) Coles, S. J.; Gale, P. A. *Chem. Sci.* **2012**, *3*, 683.
(29) *CrystalClear-SM Expert 3.1 b27*; Rigaku: TX, 2013.
(30) Palatinus, L.; Chapuis, G. *J. Appl. Crystallogr.* **2007**, *40*, 786.
(31) Sheldrick, G. M. *Acta Crystallogr.* **2008**, *A64*, 112.
(32) Williams, C. F.; Lloyd, D.; Kolarich, D.; Alagesan, K.; Duchene, M.; Cable, J.; Williams, D.; Leitsch. *Vet. Parasitol.* **2012**, *190*, 62.
(33) Mosmann, T. *J. Immunol. Methods* **1983**, *65*, 55.
(34) (a) Frank, M.; Nieger, M.; Vogtle, F.; Belser, P.; von Zelewsky, A.; de Cola, L.; Balzani, V.; Barigelletti, F.; Flamigni, L. *Inorg. Chim. Acta* **1996**, *242*, 281. (b) Juris, A.; Balzani, V.; Barigelletti, F.; Campagna, S.; Belser, P.; von Zelewsky, A. *Coord. Chem. Rev.* **1988**, *84*, 85.
(35) (a) Gudipati, V.; Curran, D. P.; Wilcox, C. S. *J. Org. Chem.* **2006**, *71*, 3599. (b) Thompson, M. K.; Doble, D. M. J.; Tso, L. S.; Barra, S.; Botta, M.; Aime, S.; Raymond, K. N. *Inorg. Chem.* **2004**, *43*, 8577.
(36) Uson, R.; Laguna, A.; Laguna, M.; Briggs, D. A.; Murray, H. H.; Fackler, J. P. *Inorganic Syntheses*; John Wiley & Sons, Inc.: New York, 2007; p 85.
(37) Steigers, C.; Olah, B.; Wuerfel, U.; Hohl-Ebinger, J.; Hinsch, A.; Haag, R. *Sol. Energy Mater. Sol. Cells* **2009**, *93*, 552.
(38) Sivkova, R.; Vohlidal, J.; Blaha, M.; Svoboda, J.; Sedlacek, J.; Zednik, J. *Macrmol. Chem. Phys.* **2012**, *213*, 411.
(39) Berchel, M.; Haelters, J.-P.; Couthon-Gourves, H.; Deschamps, L.; Midoux, P.; Lehn, P.; Jaffres, P.-A. *Eur. J. Org. Chem.* **2011**, 6294.
(40) (a) Yam, V. W.-W.; Lo, K. K.-W.; Wong, K. M.-C. *J. Organomet. Chem.* **1999**, *578*, 3. (b) Yam, V. W.-W.; Choi, S. W.-K. *J. Chem. Soc., Dalton Trans.* **1996**, 4227. (c) Ferrer, M.; Rodriguez, L.; Rosell, O.; Pina, F.; Lima, J. C.; Bardia, M. F.; Solans, X. *J. Organomet. Chem.* **2003**, *678*, 82. (d) Riva, H.; Nieuwhuyzen, M.; Fierr, C. M.; Raithby, P. R.; Male, L.; Lagunas, M. C. *Inorg. Chem.* **2006**, *45*, 1418.
(41) Albano, V. G.; Busetto, L.; Cassani, M. C.; Sabatino, P.; Schmitz, A.; Zanotti, V. *J. Chem. Soc., Dalton Trans.* **1995**, 2087.
(42) Langdon-Jones, E. E.; Symonds, N. O.; Yates, S. E.; Hayes, A. J.; Lloyd, D.; Williams, R.; Coles, S. J.; Horton, P. N.; Pope, S. J. A. *Inorg. Chem.* **2014**, *53*, 3788.
(43) Xie, J.; Chen, Y.; Yang, W.; Xu, D.; Zhang, K. *J. Photochem. Photobiol., A* **2011**, *223*, 111.
(44) Mullice, L. A.; Thorp-Greenwood, F. L.; Laye, R. H.; Coogan, M. P.; Kariuki, B. M.; Pope, S. J. A. *Dalton Trans.* **2009**, 6836.
(45) Millet, C. O. M.; Lloyd, D.; Coogan, M. P.; Rumsey, J.; Cable, J. *Exp. Parasitol.* **2011**, *129*, 17.
(46) (a) Millet, C. O. M.; Williams, C. F.; Hayes, A. J.; Hann, A. C.; Cable, J.; Lloyd, D. *Exp. Parasitol.* **2013**, *135*, 262. (b) Williams, C. F.; Millet, C. O. M.; Hayes, A. J.; Cable, J.; Lloyd, D. *Trends Parasitol.* **2013**, *29*, 311. (c) Lloyd, D.; Williams, C. F. *Mol. Biochem.* **2014**, *197*, 43.
(47) Kielar, F.; Law, G.-L.; New, E. J.; Parker, D. *Org. Biomol. Chem.* **2008**, *6*, 2256.

DOI: 10.1021/acs.inorgchem.5b00954
Inorg. Chem. 2015, 54, 6606−6615